Stability and half-metallicity of transition metal pnictides in tetrahedrally bonded structures

M. S. Miao and Walter R. L. Lambrecht
Department of Physics, Case Western Reserve University, Cleveland, Ohio 44106-7079, USA
(Received 4 June 2004; revised manuscript received 25 August 2004; published 18 February 2005)

Using a full potential linearized muffin-tin approach and the spin polarized density functional method, we studied the magnetism and the electronic structure for transition metal pnictides in the zinc blende (ZB) and the wurtzite (WZ) structures under volume expansion and compression. It was found that for many compounds the WZ structure has lower total energy than the ZB structure. The energy difference between the two tetrahedrally bonded structures are only a few meV, which indicates that the system may form other polytypes with stacking intermediate between ZB and WZ. Both ZB and WZ structure are half-metallic. There are only slight differences between ZB and WZ structures in the resulting band gaps of the minority spin and the density of states (DOS) at the Fermi level for the majority spin. This indicates that these properties are only determined by the local bonding. The minority gap and the DOS at the Fermi level are found to be strongly dependent on the volume expansion.

DOI: 10.1103/PhysRevB.71.064407 PACS number(s): 75.50.Cc, 75.90.+w, 71.20.Be, 75.75.+a

I. INTRODUCTION

Half-metallicity is defined by having a band gap for the minority spin channel and a partially filled band for the majority spin channel and has been found to occur in a number of different materials.[1–4] This profound difference in the electronic structure for both spin channels makes the half-metallic materials very promising for spin injection and spin manipulation in spintronic devices. Since its discovery in 1983,[5,6] the half-metallic state has been found in several families of materials, including the Heusler[7] and half-Heusler materials and some transition metal oxides.[8] The band gap in the minority spin channel can either arise from a complex crystal structure, as is the case in the Heusler alloys, or from strong correlation effects, as occurs in some transition metal oxides. Recently, half-metallicity has also been found to occur in transition metal compounds with simple zinc blende (ZB) but for these materials metastable structure.

Recently, some transition metal pnictides, such as CrAs,[9] CrSb,[10] and MnAs,[11] were grown as nanosize particles or thin films on certain semiconductor substrates. Although the stable structure of these compounds is usually NiAs, the nanoparticles or films were found to exhibit the ZB structure. This is caused by the large strains imposed by the substrates. This was confirmed by many recent theoretical calculations.[13–24] The calculations also showed that these compounds are half metals as their minority spin has a gap at the Fermi level and they possess an integer magnetic moment in their ferromagnetic states.

Computational investigations[13–24] showed that almost all the early transition metal pnictides and chalcogenides are half-metallic in the ZB structure and under volume expansion. Recently, Xie *et al.*[24] showed that the transition metal pnictides and chalcogenides in the WZ structure are also half-metallic under volume expansion. Although this structure has lower energy than the NiAs structure under certain volume expansion, it is unclear whether it can be a metastable structure under expansion. On the other hand, several other structures, including the NaCl structure and other tetrahedron polytype structures, have not been studied for half-metallicity under volume expansion.

The important parameters of half metals for designing a spintronics device are the gap of the minority spin bands, the density of states (DOS) of majority spin at the Fermi level and the Fermi level position relative to the conduction band minimum of minority spin. The last parameter shows the energy cost to flip an injected spin in the half metal and is also known as the spin flip gap. It is also important to see how these parameters change while we change the volume expansion. In this paper, we carefully address these problems by calculating the total energy, the electronic structure and the magnetic propeties of Mn, Cr, and V arsenides and antimonides in five different structures, including WZ, ZB, 4H, NiAs, and NaCl structures. The total energies are calculated in a hexagonal unit cell for all the structures. The **k** meshes are chosen carefully so that they are equivalent for the different structures. This specific arrangement allows us to achieve an accuracy for the energy differences of about 1 meV.

We will briefly introduce the computational method in Sec. II. In Sec. III, we present our major results, first concerning the lattice stability in Sec. III A and second concerning the magnetic and electronic properties in Sec. III B. Conclusions will be summarized in Sec. IV.

II. COMPUTATIONAL METHOD

The calculations are performed using a full potential linearized muffin-tin orbital method[25] (FPLMTO) which permits analytic calculation of the forces and hence structural optimization. This new version of FPLMTO has a number of advantages compared to earlier implementations. As usual, it divides the charge density and potential in a smooth part throughout space and a rapidly changing part inside muffin-tin spheres. The smooth part is handled accurately using a real space mesh and fast Fourier transforms. The major innovation is the use of a more efficient minimal but accurate basis set consisting of augmented "smooth Hankel" functions.[26] The smoothing is added so as to give the basis function the right curvature in the region just outside the

muffin-tin sphere radius. The parameters characterizing these features of the basis function are adjusted at the beginning of the calculation following well established procedures so as to minimize the total energy. A single set of basis functions with optimized smoothing radii and κ values already produces fairly good results. The $\kappa^2=E-V_{MTZ}$ value corresponds to the kinetic energy in the interstitial region and determines the overall fall-off of the envelope function, while the smoothing radius determines its behavior in the region between approximately the atomic Wigner-Seitz sphere radius and the smaller nearly touching muffin-tin radius inside which the basis function is as usual augmented by a solution ϕ_ν of the radial Schrödinger equation and its energy derivative $\dot{\phi}_\nu$ at a chosen linearization energy E_ν for each angular momentum l. To give additional degrees of freedom a second set of basis function is added with different smoothing radii and Hankel function energies (decay constants). We have tested that this choice is not very critical, leading to energy differences of at most 3 meV on total energies. However, for higher accuracy, we adopt two sets of basis functions for the *s*, *p*, and *d* orbitals of transition metal atoms and the *s* and *p* orbitals of group V atoms. Only one basis function is used for the group V *d* orbital. The previous version of FPLMTO requires larger basis sets because the envelope Hankel functions are not smoothed. For example, to converge the total energy differences between SiC polytypes to a few tenths of a meV required a triple κ-basis set,[32] whereas with the new FPLMTO scheme a double basis set of smoothed Hankel envelope functions sufficed.[33]

The von Barth and Hedin spin polarized exchange and correlation potential[27] is used in the local spin density functional approximation.[28,29] It is important to notice that local spin density approximation (LSDA) sometimes gives unsatisfactory results, especially for the 3*d* metals. For example, it cannot predict the correct ferromagnetic body centered cubic (bcc) ground state for iron. The generalized gradient approximation (GGA) was shown to provide an important improvement for the 3*d* metals and reproduced the correct bcc ground state for iron.[30,31] However, in the transition metal pnictides studied in this paper, the metal ions interact strongly with the surrounding anions and the 3*d* electrons are more delocalized. The LSDA is expected to perform better in such cases without gradient corrections. Indeed, the previous LSDA[12,14–17,21] calculations as well as the results in this work show good agreement on the half metalicity features, such as the critical lattice constants for half metalicity and the spin flipping gaps, with the other studies done by GGA.[19,20,22–24]

After some initial calculations, we found that the energy differences between the ZB and WZ structures are very small, only a few or a few tens of meV. Therefore one needs to be very careful with the energy convergence. Considering that the systems are metallic for the majority spin channel, a large **k**-point sampling is needed. We calculate all the structures in a hexagonally shaped unit cell. Note however, that in the ZB and RS structures, the symmetry of these unit cells is of course only triagonal, not hexagonal, when their filling with atoms is considered. The remaining symmetries of these cubic crystals are effectively ignored in these unit cells. We used a $8\times8\times4$ *k*-point mesh for the ZB and RS structures and a $8\times8\times6$ *k*-point mesh for the WZ and NiAs structures. The total energy was tested to be converged to less than 1 meV. With these choices of *k*-point meshes, the sampling points in the Brillouin zone are identical for all the structures. Using this procedure one expects the numerical errors for different structures due to the limited set of BZ sampling points used in the integration to cancel. To our knowledge this technique was first adopted in the studies of SiC polytypes. It successfully resolved the energy difference to a precision of one meV.[34]

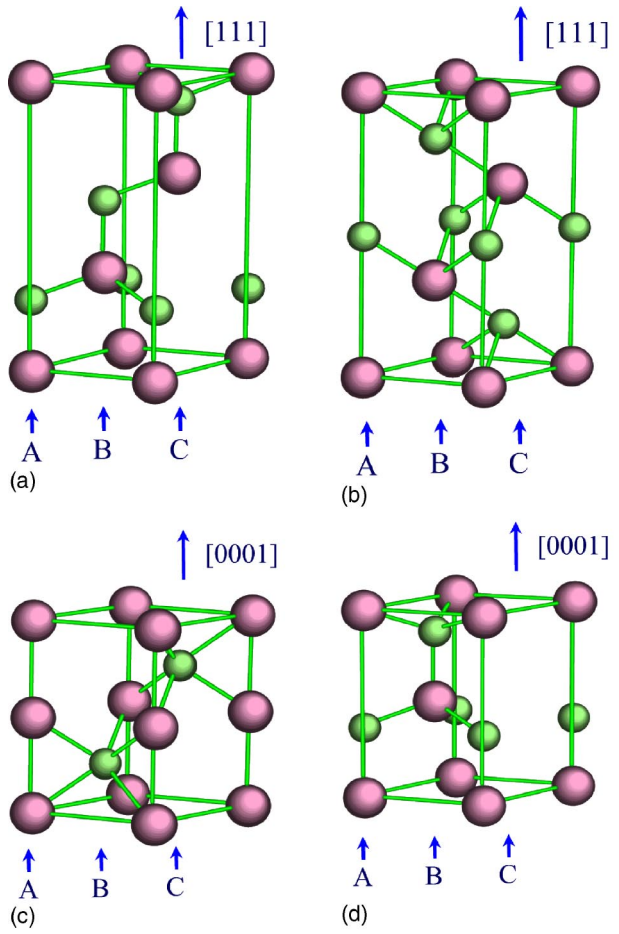

FIG. 1. (Color online) Unit cells used in this paper for ZB (top-left), NaCl (rop-right), NiAs (bottom-left), and WZ (bottom-right) structures.

Figure 1 shows the hexagonal view of the ZB and NaCl structures calculated in this paper. In the ZB structure, both cations and anions form a face centered cubic (fcc) lattice. The cations or the anions occupy the tetrahedral interstitial sites of the other sublattice. The layer sequence of fcc in the [111] direction is *ABC*. Denoting the cations in upper case letters and the anions in lower case letters, the layer sequence of ZB is *AaBbCc*. In the NaCl structure, the cations and the anions also form fcc lattices. The difference from the ZB structure is that the cations and the anions now intercalate by occupying all the octahedral interstitial sites. The layer sequence of NaCl is *AcBaCb*. In the NiAs structure, the cations form a simple hexagonal lattice whereas the anions form a hexagonal closed packed (hcp) lattice. The anions occupy

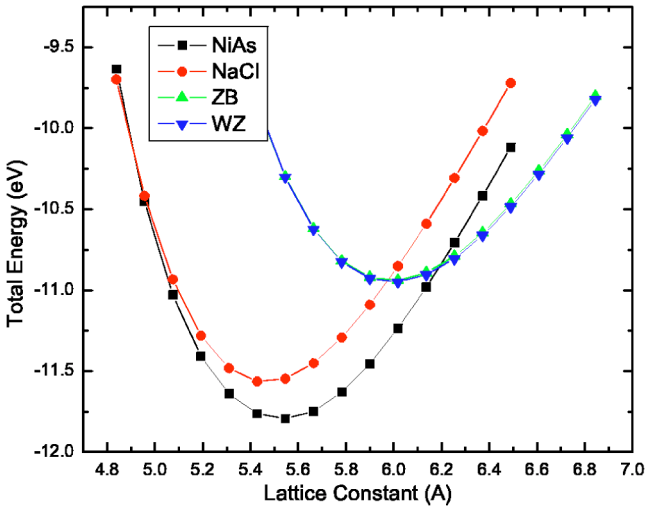

FIG. 2. (Color online) Total energy versus lattice constants CrSb in ZB, WZ, NaCl, and NiAs structure.

half of the sixfold interstitial formed by the cation sublattice. The layer sequence of NiAs is *AbAc*. The WZ structure is composed of two hcp lattices in which each occupies the tetrahedral interstitial sites of the other sublattice. The layer sequence is *AaBbAaBb*. Both ZB and WZ structures are fourfold coordinated whereas the NaCl and the NiAs structures are sixfold coordinated. The local bonding of WZ is very similar to ZB except that the symmetry is lower for the WZ structure and one of the four bonds (along the *c* axis) is slightly different from the other three. This will result in a different splitting of the *d* orbitals of the cations caused by the crystal field interaction with the surrounding anions.

III. RESULTS

A. Stability of WZ and ZB structures

The volume dependence of the total energies for the various systems looks quite similar. We here only present the data for CrSb in Fig. 2. The total energy shown is actually the energy relative to that of the atoms infinitely far apart, in other words, minus the cohesive energy, and is normalized per formula unit. It can be seen that the NiAs structure is the most stable one for CrSb. With no compression or expansion, the material favors the sixfold coordinated structures, especially the NiAs structure. Under certain volume compression (external pressure), there is a phase transition from the NiAs to the NaCl structure. The changes of the structure from NiAs to NaCl under pressure are the result of the fact that the NaCl structure is more closely packed than the NiAs structure. The high symmetric way of arranging the positive and negative charges in NaCl structure also lowers the Madelung energy. On the other hand, the fourfold coordinated structures are all much higher in energy than the sixfold coordinated structures under ambient condition and compression. Only under large volume expansion, these structures could become metastable. Such metastable structures have been found for CrAs, CrSb, and MnAs in nanosized particles or very thin films grown on semiconductor substrates. The mismatch with the substrate lattice causes large strains to the films and the nanoparticles. Beyond a certain critical volume, however, this strain cannot be maintained and misfit dislocations would appear. The energy difference is about 0.7 eV per formula unit. The transition volume from the NiAs to the ZB structure, i.e., the volume where the two energy-volume curves cross, is 59.6 $Å^3$/formula. These values are in good comparison to the previous calculations.[23] Most interestingly, the WZ structure shows a slightly lower energy than the ZB structure under large volume expansion.

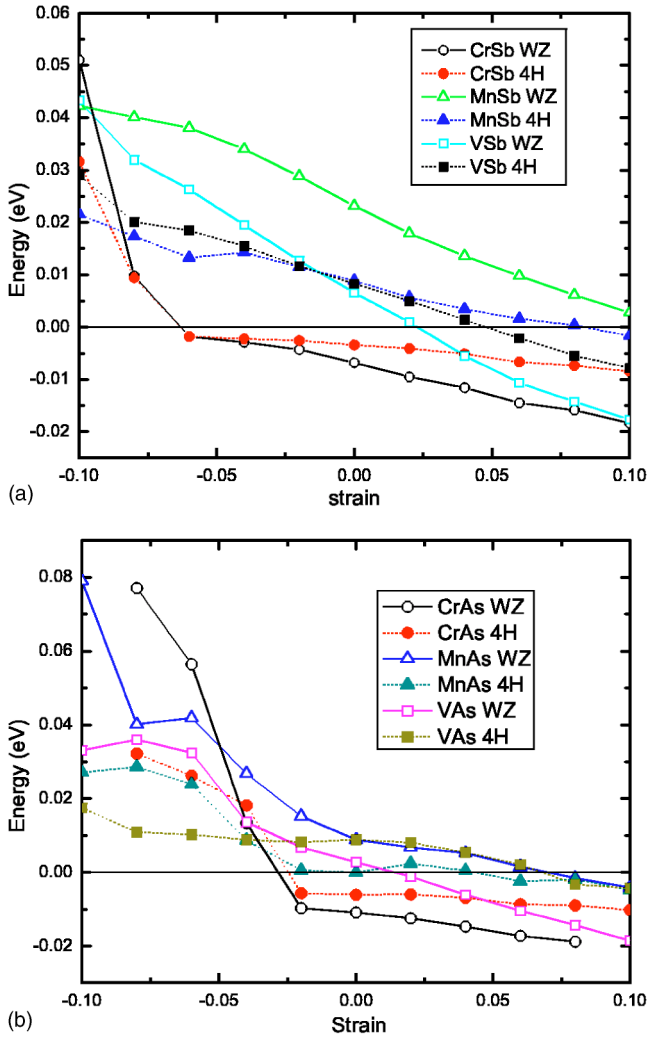

FIG. 3. (Color online) Relative total energy with respect to ZB for WZ and 4H structures for VAs, VSb, CrAs, CrSb, MnAs, and MnSb. The isotropic strain ($\Delta a/a$) is relative to the equilibrium values of the ZB structure.

To find the metastable structure under volume expansion, we present the total energies for VSb, CrSb, and MnSb under various volume expansions in Fig. 3(a) and the total energies for VAs, CrAs, and MnAs in Fig. 3(b). The energies are depicted for the WZ and 4*H* structures relative to those for the ZB structure. 4*H* is a denotation for one of the SiC polytypes that consists of 50% hexagonal layers and 50% cubic layers. The layer sequence for 4*H* is *AaBbCcBb*. For SiC, the WZ structure is the most unstable one with energy of 3 meV higher than the ZB structure. The 4*H* is most stable

and is lower in energy than ZB by about 1.5 meV.[32,34] As shown by Fig. 3, under a compressed volume (relative to the equilibrium of the ZB structure) the ZB structure is the most stable fourfold coordinated structure for all the studied pnictides. While the volume expands, the WZ and 4*H* structures become more and more stable relative to the ZB structure. CrSb is metastable in the WZ structure for a volume smaller than the equilibrium ZB. VSb is stable in WZ structure under a slight volume expansion relative to the ZB one. For MnSb, the WZ structure is not stable in the range of volume expansion calculated in this paper. At a lattice expansion of about 6%, the 4*H* structure becomes the metastable one for MnSb.

The arsenides have a similar tendency as the antimonides. For CrAs, the WZ and 4*H* structures are lower in energy than the ZB structure at a volume even smaller than the equilibrium volume for ZB structure. The energy difference between the WZ and the ZB structure can be as large as 20 meV. VAs becomes metastable in the WZ structure at a volume slightly larger than the equlibrium volume for the ZB structure. The energy of the WZ structure for MnAs only becomes lower than that of the ZB structure at about 7% lattice expansion relative to the equlibrium lattice constant for the ZB structure. However, its 4*H* structure is very close in energy to the ZB structure at the ZB equilibrium volume.

Most of the density functional calculations for transitional metal pnictides so far, including the present one, were carried out under the assumption of uniform lattice expansions. However, in thin film or particle growth upon a substrate, there should be a large biaxial distortion accompanying the isotropic one considered here. One may assume that the cubic ZB structure is favored relative to the hexagonal NiAs structure while grown on the (100) planes of a ZB semiconductor substrate not only because of the expansion favoring the metastable structure but also because of the continuity of the bonding with the substrate. It is not so clear that this will happen for the WZ because the latter shares hexagonal symmetry with the NiAs structure. However, one may expect that for growth on a (111) plane substrate with sufficiently larger in-plane lattice constant the WZ could still be favored because it has lower energy. The biaxial strain effects on the energy will require further study.

B. The half-metallicity of WZ and ZB structures

To check the half-metallicity and other magnetic properties, we calculated the magnetic moments for all the compounds in the different structures here considered. Figure 4 shows the results for CrSb. The magnetic moments for the other compounds have similar tendency as shown in Fig. 4 and therefore are not shown in this paper. From Fig. 4, one can see that both the ZB and WZ structures start to have integer magnetic moments at a lattice constant of 5.6 Å, which is a good indication of half-metallicity. By checking the corresponding band structure and DOS, we confirmed that they are in the half-metallic state. The critical volume for half-metallicity is evidently smaller than the equilibrium volumes for both WZ and ZB structures, indicating that the half-metallicity is strong in CrSb. It is worth to notice that the NaCl and NiAs structures can possess a magnetic moment larger than that of the half metal, which is a result of the strong spin polarization.

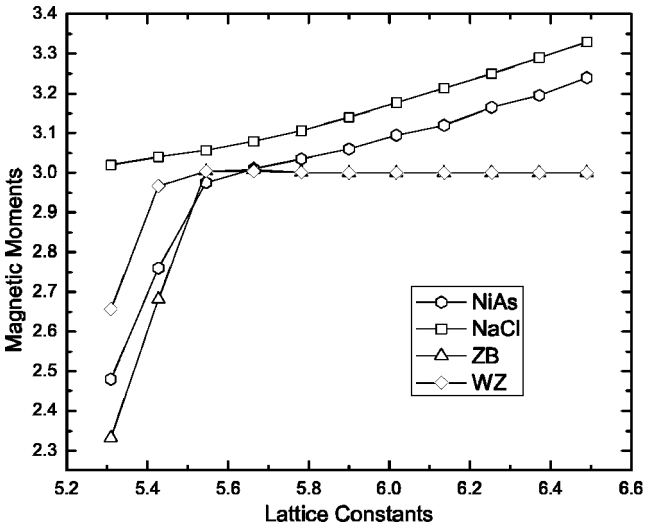

FIG. 4. The magnetic moment of CrSb under volume compression and expansion and in NiAs, NaCl, ZB, and WZ structures.

Our results of half-metallicity in WZ structure and under volume expansion agree with the previous theoretical results.[20] These results indicate that the half-metallicity is mainly caused by the local bonding environment. It is the result of a competition between the spin splitting and the crystal field splitting that is mainly caused by the local bonding. For both ZB and WZ structure, the local tetrahedral bonding splits the *d* orbitals into t_2 and *e* states. Only t_2 states have strong coupling with the surrounding *p* orbitals of the anions and form the bonding and antibonding states.

Figure 5 shows the band structure of CrSb in ZB and WZ structures. In both structures the minority spin bands have a gap. Let us first look at the bands of the ZB structure. The lowest three bands for both majority and minority spins are the bonding t_2-*p* states and are mainly composed of anion *p* orbitals. These bands are deep in the valence band. The next two bands are formed by *e* states. The majority *e* bands are lying in the valence bands whereas the minority *e* states in the conduction bands. These bands are fairly narrow compared with the t_2 bands consistent with the nonbonding nature of the *e* states. The t_2 bands have a larger band width because these orbitals have indirect interactions between them via the Sb *p* states. The large spin polarization of the *e* states arises because these bands are narrow and atomiclike and is the origin of the gap for minority spins and therefore the origin of the half-metallicity. The antibonding t_2-*p* bands of majority spin are partially filled and are the bands that cross the Fermi level. The corresponding bands for minority spin are high in the conduction bands.

In the ZB symmetry, the t_2-*p* bands are threefold degenerate at the Γ point and twofold degenerate along the Γ-*L* line. The *e* states are twofold degenerate at the Γ point and twofold degenerate along the Γ-*L* line. Of course, strictly speaking the t_2 and *e* labels strictly apply only at the Γ point where the point group is T_d. At general **k** points in the BZ, these orbitals mix but still the bands that we designate as *e* or t_2 symmetry consist predominantly of the corresponding

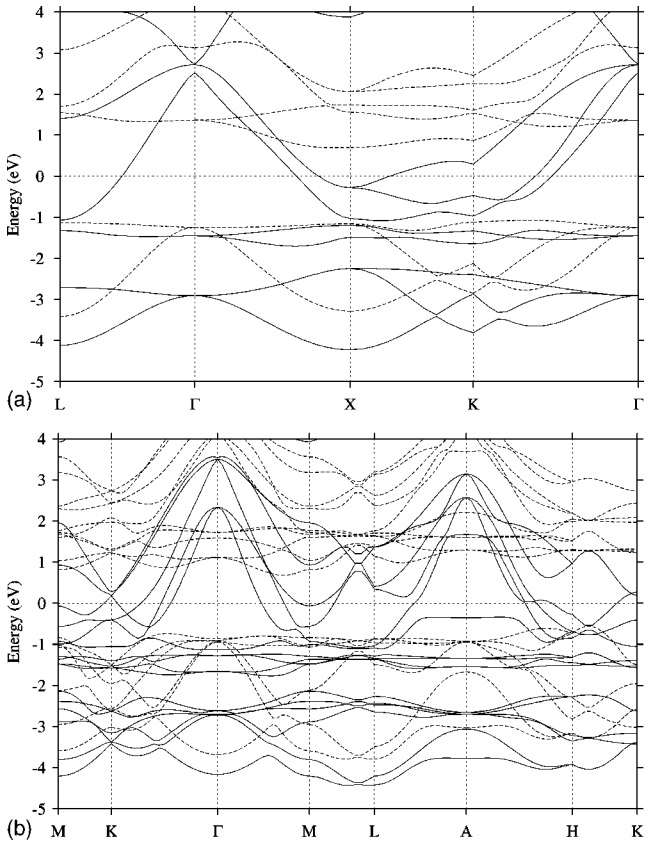

FIG. 5. The band structure for CrSb in (a) ZB (b) WZ structures and with a lattice constants of 5.9 Å. Solid lines: majority spin, dashed lines: minority spin.

atomic orbitals in a linear combination of atomic orbitals picture. In the WZ band structure, the groups of the e and t_2-p bands can still be distinguished. However, due to the breaking of the tetrahedral symmetry, the degeneracy of the bands at high symmetric points and lines in the BZ is broken. For example, the threefold degenerate t_2-p bonding and antibonding states at the Γ point each split into a twofold e_1 symmetric state and a nondegenerate a_1 symmetric state using the symmetry labels for the C_{6v} point group. These correspond to the irreducible representations which transform as x,y orbitals and z orbitals at the origin, respectively.

The important electronic features of a half-metallic material include (1) the minority band gap $E_g^{\downarrow}$, (2) the minority spin valence band maximum (VBM) relative to the Fermi level, (3) the minority spin conduction band minimum (CBM) also relative to the Fermi level, also known as the spin-flip gap E_g^{sp}, and (4) the DOS $N_{\uparrow}(E_F)$ of the majority spin at the Fermi level. These features are listed in Table I for all six compounds calculated in this paper. They are all obtained at the same cubic lattice constant, 6.06 Å which is the lattice constant for InAs. For the WZ structures this means that we use $a_h = a_c/\sqrt{2}$ as hexagonal in-plane lattice constant. For comparison, both the ZB and the WZ structure parameters are listed. It is evident that these features are very similar for the two different structures, indicating that they are mainly determined by the local bonding. We also include in this table the equilibrium lattice constant a_0 and the critical cubic lattice constant a_{cr} at which half-metallicity appears first.

TABLE I. Equilibrium lattice constants (a_0 in Å), critical lattice constants (a_{cr} in Å), VBM ($E_{\mathrm{VBM}}-E_F$), CBM or spin-flip-gap ($E_g^{\mathrm{sp}}=E_{\mathrm{CBM}}-E_F$), minority band gap $E_g^{\downarrow}$, all energies in eV and majority DOS $N_{\uparrow}(E_F)$ at the Fermi level in states per eV per spin per cell.

		a_0	a_{cr}	VBM	CBM	$E_g^{\downarrow}$(eV)	DOS
VAs	ZB	5.6	5.4	−1.37	1.07	2.44	∼0
	WZ	5.6	5.4	−1.29	1.06	2.35	∼0
VSb	ZB	6.0	5.6	−1.30	0.89	2.19	∼0
	WZ	6.0	5.5	−1.25	0.90	2.15	∼0
CrAs	ZB	5.4	5.5	−1.24	1.28	2.52	0.60
	WZ	5.4	5.4	−1.17	1.35	2.52	0.83
CrSb	ZB	6.0	5.8	−1.2	0.99	2.19	0.60
	WZ	6.0	5.8	−1.14	1.09	2.23	0.65
MnAs	ZB	5.4	5.8	−1.32	0.74	2.06	0.4
	WZ	5.4	5.8	−1.34	0.68	2.02	0.26
MnSb	ZB	6.0	6.0	−1.41	0.35	1.76	0.24
	WZ	6.0	6.0	−1.41	0.35	1.76	0.24

The electronic structure for NaCl structure is totally different from those for ZB and WZ structures, because of the difference in local bonding. In the NaCl structure, the e_g states couple strongly with the anion p states and form bonding and antibonding e_g-p states. We now use the labels for the octahedral group O_h which are either even (g) or odd (u) with respect to inversion. Now, the t_{2g} states are nonbonding. Figure 6 shows the DOS for CrSb in NaCl, ZB, and WZ structures and with lattice constant of 5.9 Å. The DOS for ZB and WZ structures shows clearly a gap for the minority spin channel. However, for the NaCl structure, there is a small but nonzero value in DOS between the nonbonding t_{2g} and the bonding e_g-p states of minority spin channel. Therefore, the band structure in the NaCl structure is not half-metallic. For the majority spin in the NaCl structure, the Fermi level can lie in the antibonding e_g-p states under large volume expansion. Therefore the RS magnetic moment can be larger than that of the corresponding ZB half metal (see Fig. 4).

C. Volume dependence of half-metallicity

The half-metallic properties strongly depend on the lattice expansion. Most of the transition metal pnictides are only half-metallic under a large lattice expansion. They are not half-metallic while the lattice constants are smaller than a critical value, although most of them are still ferromagnetic. Two possible changes in the electronic structure may cause the reduction of the half-metallicity, namely the reduction of the band gap for minority spin and the changes of the Fermi level relative to the CBM of minority spin.

In Fig. 6, we presented the DOS of CrSb at a lattice constant above the critical value a_{cr} for half-metallicity. For comparison, Fig. 7 shows the DOS at a lattice constant below the critical value. In the former case, the Fermi level

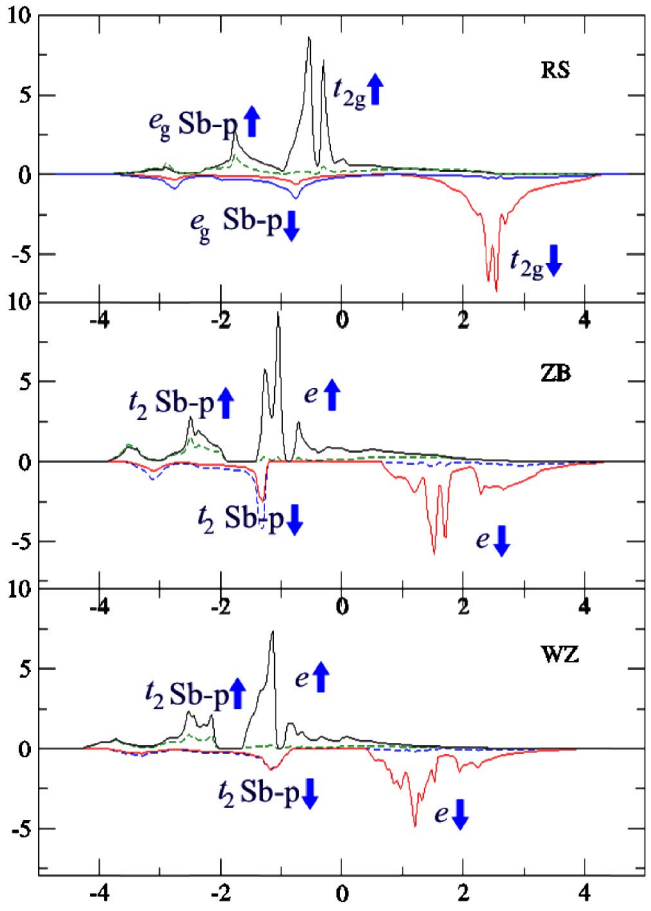

FIG. 6. (Color online) PDOS for CrSb in NaCl, ZB, and WZ structures and with lattice constants of 5.9 Å. Black solid line: Mn *d* majority spin, red dashed line: Mn *d* minority spin, green dotted line: N *p* majority spin, and blue dash-dotted line: N *p* minority spin.

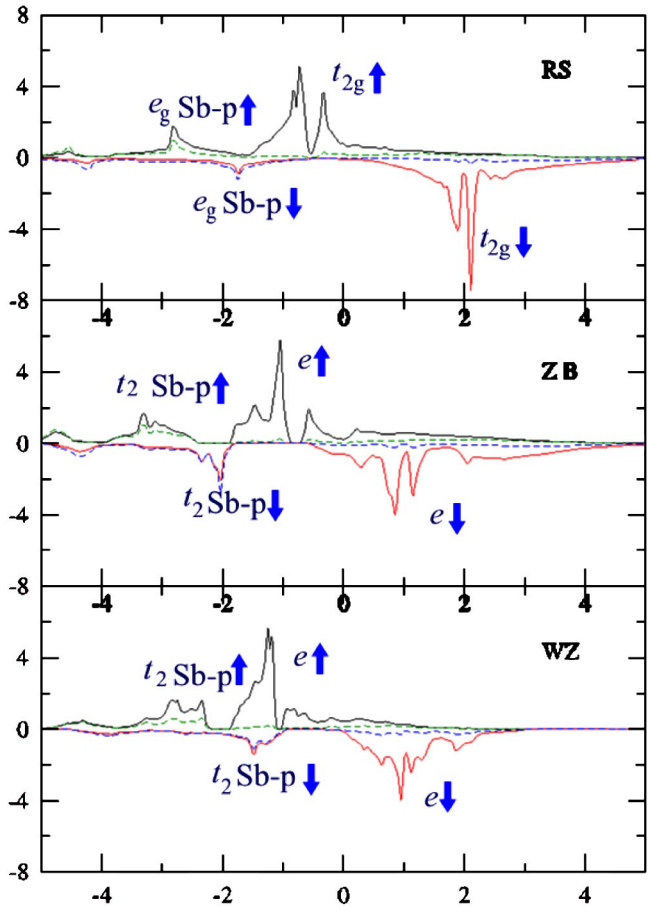

FIG. 7. (Color online) DOS for CrSb in NaCl, ZB, and WZ structures and with lattice constants of 5.3 Å. Black solid line: Mn *d* majority spin, red dashed line: Mn *d* minority spin, green dotted line: N *p* majority spin, blue dash-dotted line: N *p* minority spin.

locates deep inside the gap of minority spin bands and therefore the system is half-metallic. With decreasing lattice constant, the gap of the minority spin becomes smaller. Meanwhile the Fermi level position also changes toward the CBM and is inside the minority conducting bands for a subcritical value of the lattice constant.

For clarifying the changes of the electronic structure versus the lattice constant, we calculated the minority band gap and the Fermi level position for CrSb as function of lattice constant. The results are plotted in Fig. 8. The connected stairs line shows the minority band gap, or the minority spin conduction band minimum relative to the minority spin valence band maximum taken as zero energy reference. The unconnected lines show the Fermi level position relative to the VBM of minority spin. It clearly reveals the gradual decrease of the minority band gap and the increase of the Fermi level with decreasing lattice constant. The changes are almost linear for both parameters. At a lattice reduction of about 7% for CrSb, the two values cross, indicating that the spin flip gap is zero and the system has lost its half-metallicity. Meanwhile, the DOS at the Fermi level decreases which is a result of the broadening majority bands.

The changes of the bands versus lattice constant can be understood by the change in bonding and the changes of the spin splitting. The change of the minority gap is totally different from the usual change of a semiconductor gap under compression. A typical semiconductor gap will become larger under compression due to the stronger coupling between neighboring atoms that will increase the gap between bonding and antibonding states. For transition metal pnictides, however, the gap of the minority spin bands is determined mainly by the spin splitting of the *e* states and the position of the Fermi level relative to the minority spin bonding t_2-*p* states. While the lattice constant decreases, the strong bonding will delocalize the *d* electrons and therefore reduce their spin splitting. This reduces the minority spin gap. On the other hand, the compression will also increase the splitting between the bonding t_2-*p* states and the antibonding t_2-*p* states. Therefore the Fermi level that locates in the antibonding t_2-*p* states is pushed up. The broadening of the antibonding t_2-*p* bands caused by the delocalization of the *d* electrons also moves up the Fermi level.

The strains required to obtain half metallicity are usually very small. As shown in Table I, except MnAs, all the other calculated asernides and antimonides start to be half-metallic at a lattice constant smaller or near their equilibrium values. On the other hand, as shown in this section, the larger the lattice constants, the bigger the spin flip gaps and therefore

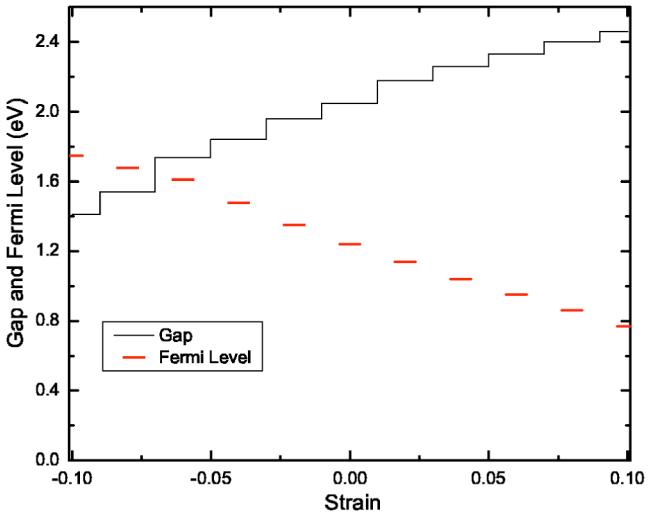

FIG. 8. (Color online) Changes of the minority gap and the Fermi level position with strain.

the better half-metallicity. However, very large strains may not be achievable without significant strain-relieving distortions of the system. The issue of which strains are sustainable requires a specific examination for each interface system of interest. The strains at the interface should also be nonisotropic. A further study of these aspects is outside the scope of this paper and postponed to future work.

IV. CONCLUSIONS

In this paper, we calculated the electronic and magnetic properties of six transition metal pnictides including CrAs, CrSb, MnAs, MnSb, VAs, and VSb. The calculations are done for several structures, including the NiAs, NaCl, WZ, ZB, and 4*H* structures. We found that under lattice expansion, the fourfold structures become metastable. Especially for several compounds, the WZ structure or the 4*H* structure can have the lowest energy under certain lattice expansion. All the fourfold structures are found to be half-metallic under expansion. The major features, such as the minority band gap, the Fermi level position, and the majority spin DOS at the Fermi level, are very close for the different fourfold structures. The breaking of the tetrahedral symmetry in WZ structure has evident effects on the band structure. While the volume increases, the minority band gap increases and the relative Fermi level position to the VBM of minority spin decreases. This is different from a typical semiconductor band gap dependence on the volume and is caused by the exchange interaction between the majority and the minority spins that will increase with the expansion of the volume. The same effect also causes a slight increase of the DOS for majority spin at the Fermi level.

ACKNOWLEDGMENTS

This work was supported by the Office of Naval Research under Grant No. N00014-02-0880 and the National Science Foundation under Grant No. ECS-0223634. Most of the calculations were performed on the Beowulf AMD cluster at the Ohio Supercomputing Center and supported under Project No. PDS0145.

[1] D. D. Awschalom and J. M. Kikkawa, Phys. Today **52**(6), 33 (1999).
[2] S. A. Wolf, D. D. Awschalom, R. A. Buhrman, J. M. Daughton, S. von Molnár, M. L. Roukes, A. Y. Chtchelkanova, and D. M. Treger, Science **294**, 1488 (2001).
[3] I. S. Osborne, Science **294**, 1483 (2001).
[4] W. E. Pickett and J. S. Moodera, Phys. Today **54**(5), 39 (2001).
[5] R. A. de Groot, F. M. Mueller, P. G. van Engen, and K. H. J. Buschow, Phys. Rev. Lett. **50**, 2024 (1983).
[6] R. A. de Groot, Physica B **172**, 45 (1991).
[7] C. Palmstrom, Mater. Res. Bull. **28**, 725 (2003).
[8] J. M. D. Coey and C. L. Chen, Mater. Res. Bull. **28**, 720 (2003).
[9] H. Akinaga, T. Manago, and M. Shirai, Jpn. J. Appl. Phys., Part 2 **39**, L1118 (2000).
[10] J. H. Zhao, F. Matsukura, K. Takamura, E. Abe, D. Chiba, and H. Ohno, Appl. Phys. Lett. **79**, 2776 (2001).
[11] K. Ono, J. Okabayashi, M. Mizuguchi, M. Oshima, A. Fujimori, and H. Akinaga, J. Appl. Phys. **91**, 8088 (2002).
[12] M. Shirai, Physica E (Amsterdam) **10**, 143 (2001).
[13] P. Ravindran, A. Delin, P. James, B. Johansson, J. M. Wills, R. Ahuja, and O. Eriksson, Phys. Rev. B **59**, 15 680 (1999).
[14] S. Sanvito and N. A. Hill, Phys. Rev. B **62**, 15 553 (2000).
[15] A. Continenza, S. Picozzi, W. T. Geng, and A. J. Freeman, Phys. Rev. B **64**, 085204 (2001).
[16] Y. J. Zhao, W. T. Geng, A. J. Freeman, and B. Delley, Phys. Rev. B **65**, 113202 (2002).
[17] Y.-Q. Xu, B.-G. Liu, and D. G. Pettifor, Phys. Rev. B **66**, 184435 (2002).
[18] I. Galanakis, P. H. Dederichs, and N. Papanikolaou, Phys. Rev. B **66**, 134428 (2002).
[19] B.-G. Liu, Phys. Rev. B **67**, 172411 (2003).
[20] W.-H. Xie, Y.-Q. Xu, B.-G. Liu, and D. G. Pettifor, Phys. Rev. Lett. **91**, 037204 (2003).
[21] I. Galanakis and P. Mavropoulos, Phys. Rev. B **67**, 104417 (2003).
[22] J. E. Pask, L. H. Yang, C. Y. Fong, W. E. Pickett, and S. Dag, Phys. Rev. B **67**, 224420 (2003).
[23] B. Sanyal, L. Bergqvist, and O. Eriksson, Phys. Rev. B **68**, 054417 (2003).
[24] W.-H. Xie and B.-G. Liu, and D. G. Pettifor, Phys. Rev. B **68**, 134407 (2003).
[25] M. Methfessel, M. van Schilfgaarde, and R. A. Casali, in *Electronic Structure and Physical Properties of Solids, The uses of the LMTO Method*, edited by Hugues Dreyssé, Springer Lecture Notes, Workshop Mont Saint Odille, France, 1998 (Springer, Berlin, 2000), p. 114–147.

[26] E. Bott, M. Methfessel, W. Krabs, and P. C. Schmidt, J. Math. Phys. **39**, 3393 (1998).
[27] U. von Barth and L. Hedin, J. Phys. C **5**, 2064 (1972).
[28] P. Hohenberg and W. Kohn, Phys. Rev. **136**, B864 (1964).
[29] W. Kohn and L. J. Sham, Phys. Rev. **140**, A1133 (1965).
[30] C. Amador, W. R. L. Lambrecht, and B. Segall, Phys. Rev. B **46**, 1870 (1992).
[31] V. Ozoliņš and M. Körling, Phys. Rev. B **48**, 18 304 (1993).
[32] S. Limpijumnong and W. R. L. Lambrecht, Phys. Rev. B **57**, 12 017 (1998).
[33] M. S. Miao (unpublished).
[34] C. Cheng, R. J. Needs, and V. Heine, J. Phys. C **21**, 1049 (1988).